

## Kinematics of Molecular Hydrogen Emission from Planetary and Pre-planetary Nebulae

Joel H. Kastner, Ian Gatley

*Chester F. Carlson Center for Imaging Science, Rochester Institute of Technology, 54 Lomb Memorial Dr., Rochester, NY 14623*

David A. Weintraub

*Dept. of Physics & Astronomy, Vanderbilt University, Nashville, TN*

### Abstract.

We report results from a program of high-resolution spectral mapping of rotational H<sub>2</sub> emission from bipolar planetary and pre-planetary nebulae. Long-slit spectra obtained with the NOAO Phoenix near-infrared spectrometer allow us to probe the molecular kinematics of these nebulae at moderate spatial resolution. We find strong evidence of a component of rotation in the equatorial H<sub>2</sub> emission from the Egg nebula (RAFGL 2688). In this nebula and in the pre-planetary nebula RAFGL 618, the H<sub>2</sub> kinematics point to the recent emergence of high-velocity polar flows, which likely mark the fairly sudden terminations of the red giant phases of their central stars. The classical bipolar planetary NGC 2346 displays distinct kinematic components, which we interpret as arising in the morphologically distinct equatorial and polar regions of the nebula. The H<sub>2</sub> rings observed in the Phoenix position-velocity maps of this nebula support the hypothesis that ring-like planetaries that display H<sub>2</sub> emission possess bipolar structure.

### 1. Introduction

The presence of molecular hydrogen emission is now recognized as a reliable indicator of bipolar structure in planetary nebulae (Zuckerman & Gatley 1988; Kastner et al. 1994, 1996). While the polar lobes often display H<sub>2</sub>, the molecular emission is, with few exceptions, brightest toward the waists of bipolar planetaries. These molecule-rich regions of planetary nebulae (PNs) appear to be the remnants of circumstellar disks or tori formed during previous, asymptotic giant branch (AGB) or post-AGB phases of the central stars. Furthermore, the available evidence suggests that the onset of H<sub>2</sub> emission postdates the AGB stage but precedes the formation of the PN (Weintraub et al. 1998). This onset likely signals the beginning of a high-velocity, collimated, post-AGB wind, which shocks the previously ejected, “slow,” AGB wind and thereby produces the observed H<sub>2</sub> emission (Kastner et al. 1999).

These observations make clear that further investigations of H<sub>2</sub> emission are important to our understanding of the origin of bipolarity in PNs. It is of

particular interest to establish whether the spatially distinct waist and lobe H<sub>2</sub> emission regions are kinematically distinct as well and, furthermore, whether the kinematics bear evidence of the presence of circumstellar disks and/or high-velocity polar flows. To this end, we have undertaken a program of spectroscopic mapping of near-infrared H<sub>2</sub> emission from planetary and pre-planetary nebulae at high spectral resolution. First results from this program were presented in Weintraub et al. (1998), in which H<sub>2</sub> emission was detected from a pair of bipolar pre-planetary nebulae (PPNs), and in Kastner et al. (1999), where we described preliminary results for the seminal PPN RAFGL 2688. Here we present further analysis and interpretation of H<sub>2</sub> velocity mapping of RAFGL 2688, as well as H<sub>2</sub> velocity mapping results for the PPN RAFGL 618 and the bipolar planetary nebula NGC 2346 (see also Arias & Rosado, in this volume).

## 2. Observations

Data presented here were obtained with the NOAO<sup>1</sup> Phoenix spectrometer on the 2.1 m telescope at Kitt Peak, AZ, in 1997 June (RAFGL 2688) and 1997 December (RAFGL 618, NGC 2346). Phoenix illuminates a  $256 \times 1024$  section of an Aladdin InSb detector array. The spectrograph slit was  $\sim 60'' \times 1.4''$  oriented approximately east-west. The velocity resolution was  $\sim 4 \text{ km s}^{-1}$  and the spatial resolution  $\sim 1.5''$  at the time these spectra were obtained. A spectral image centered near the  $2.121831 \mu\text{m } S(1), v = 1 - 0$  transition of H<sub>2</sub> was obtained at each of 12 spatial positions as the slit was stepped from south to north across RAFGL 2688. The step size,  $1.0''$ , provided coverage of the entire H<sub>2</sub> emitting region with spatial sampling approximating the slit height. For RAFGL 618, whose bright H<sub>2</sub> emission regions are oriented almost perfectly east-west (Latter et al. 1995), parallel to the Phoenix slit, we obtained a single spectral image centered on the object. For NGC 2346 we obtained spectral images at selected positions near the waist of the nebula. Spectral images were reduced and wavelength calibrated as described in Weintraub et al. (1998). For the RAFGL 2688 data, the reduced spectral images were stacked in declination according to the commanded telescope offsets, to produce a (RA, dec, velocity) data cube of H<sub>2</sub> emission.

## 3. Results and Discussion

### 3.1. RAFGL 2688

Kastner et al. (1999) presented selected velocity planes from the RAFGL 2688 Phoenix data cube. The four principal “lobes” of H<sub>2</sub> emission seen in direct H<sub>2</sub> images (e.g., Sahai et al. 1998) are also apparent in these Phoenix data, with one pair oriented parallel to the polar axis (roughly N-S) and one perpendicular (roughly E-W). Each of these H<sub>2</sub> lobe pairs displays a velocity gradient, with the N and E lobes blueshifted by up to  $\sim 30 \text{ km s}^{-1}$  and the S and W lobes

---

<sup>1</sup>National Optical Astronomy Observatories is operated by Associated Universities for Research in Astronomy, Inc., for the National Science Foundation.

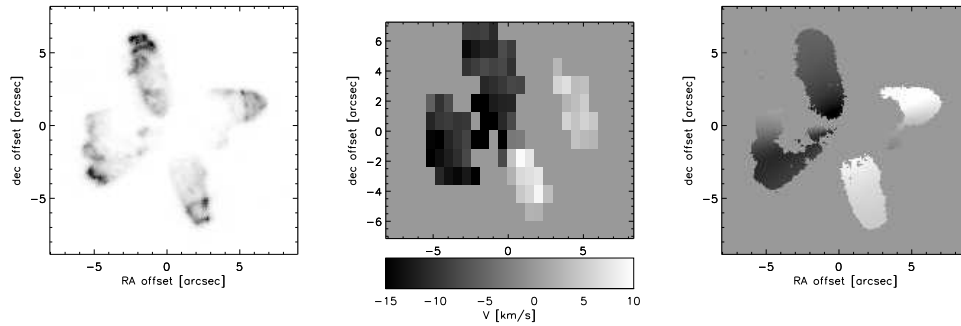


Figure 1. Comparison of the model and observed  $H_2$  velocity fields of RAFGL 2688. The velocity greyscale bar applies to the center and right panels. The HST/NICMOS  $H_2$  image (Sahai et al. 1998) is shown at left. The observed velocity field (center) consists of velocity centroids calculated from the Phoenix data cube. In the model (right), we set the equatorial expansion velocity at  $v_e = 5 \text{ km s}^{-1}$  and the equatorial rotation velocity at  $v_r = 10 \text{ km s}^{-1}$ . The comparison indicates that there is reasonable qualitative and quantitative agreement between model and data for this choice of parameters.

similarly redshifted. However, the N-S and E-W H<sub>2</sub> lobe pairs differ in their detailed kinematic signatures (Kastner et al.).

The H<sub>2</sub> kinematic data for RAFGL 2688, like velocity maps obtained from radio molecular line emission, can be described in terms of a multipolar system of purely radially directed jets (Cox et al. 1997; Lucas et al., these proceedings). Given the constraints imposed by Phoenix and *Hubble Space Telescope* data, however, this model would require that the “equatorial” components located east and west of the central star are in fact directed well above and below the equatorial plane, respectively (Kastner et al. 1999). If one postulates instead that the E-W H<sub>2</sub> emission lobes are confined to the equatorial plane of the system — a hypothesis that appears to be dictated by certain details of the H<sub>2</sub> surface brightness distribution, as well as by simple symmetry arguments — then one must invoke a model combining radial expansion with a component of azimuthal (rotational) velocity along the equatorial plane (Kastner et al.). In a forthcoming paper we will compare these two alternative models in more detail. Here, we describe a specific formulation of the latter (expansion + rotation) model that reproduces many of the salient features of the Phoenix data.

To construct this empirical model of the H<sub>2</sub> kinematics of RAFGL 2688, we are guided by the basic results described above. That is, the polar lobes are characterized by velocity gradients in which the fastest moving material is found closest to the star, and the slowest moving material is found at the tips of the H<sub>2</sub> emission regions. For simplicity, we assume this behavior can be described by an inverse power law relationship between velocity and radius. For the equatorial plane H<sub>2</sub> emission, meanwhile, we assume a combination of azimuthal (rotation) and radial (expansion) velocity components, whose magnitudes we denote by  $v_r$  and  $v_e$ , respectively.

To constrain these model parameters, we compared model velocity field images with a velocity centroid image which we obtained from the Phoenix data cube. For the polar lobes, we find that the exponent of the inverse power law velocity-distance relationship is roughly  $\sim 0.7$  and that the outflow velocities at the tips of the N and S lobes are  $\sim 20$  km s<sup>-1</sup>. For the equatorial regions, good agreement between model and data is obtained for values of  $v_e$  and  $v_r$  that lie in the range 5 – 10 km s<sup>-1</sup>, with the additional constraint  $v_e + v_r \sim 15$  km s<sup>-1</sup>. An example of the results for a representative model (with  $v_e = 5$  km s<sup>-1</sup> and  $v_r = 10$  km s<sup>-1</sup>) is displayed in Fig. 1. There is clear qualitative agreement between the model and observed velocity images for these parameter values, in the sense that the overall distribution of redshifted and blueshifted emission is captured by the model. Furthermore, this model reproduces specific details of the observed H<sub>2</sub> velocity distribution, such as the approximate magnitudes and positions of the velocity extrema in the four H<sub>2</sub> lobes. While this model is by no means unique, the comparison of calculated and observed velocity fields provides further support for a component of azimuthal velocity along the equatorial plane of RAFGL 2688, and offers an indication of the magnitude of this “rotational” component relative to the components of radial expansion both parallel and perpendicular to the polar axis of the system.

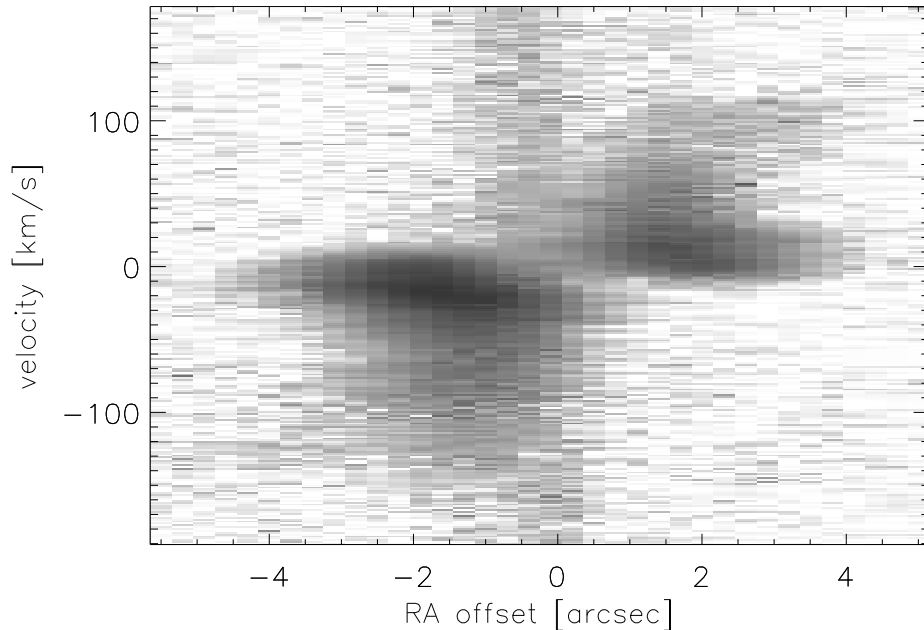


Figure 2. Phoenix spectral image of RAFGL 618. The velocity scale of the image is centered on the systemic velocity of RAFGL 618. East is to the left. The image is displayed in a logarithmic greyscale to bring out the line wing emission, which extends to at least  $\sim \pm 100 \text{ km s}^{-1}$ . The vertical band across the image at RA offset  $\sim 0''$  is produced by continuum emission from the vicinity of the central star.

### 3.2. RAFGL 618

The Phoenix spectral image obtained for RAFGL 618 is displayed in Fig. 2. Bright H<sub>2</sub> emission is detected along the entire polar axis of RAFGL 618. These data demonstrate further that very high velocity H<sub>2</sub> emission is present in this bipolar outflow. The highest velocity molecular material is found closest to the central star of RAFGL 618. We conclude that the velocity gradients along the polar axes of both RAFGL 2688 and RAFGL 618 trace rapid transitions from the “slow,” spherically symmetric winds of their AGB progenitors to faster, collimated, post-AGB winds (Kastner et al. 1999).

### 3.3. NGC 2346

In Fig. 3 we display an H<sub>2</sub> image of NGC 2346 obtained with the NOAO Cryogenic Optical Bench (Kastner et al. 1996) and we illustrate the slit positions used for Phoenix spectroscopic observations. Phoenix spectral images of NGC 2346 obtained at these positions are presented in Fig. 4. These images demonstrate that the H<sub>2</sub> emission from the bipolar NGC 2346 forms rings or ellipses in position-velocity space, an observation that reinforces our prior conclusion that

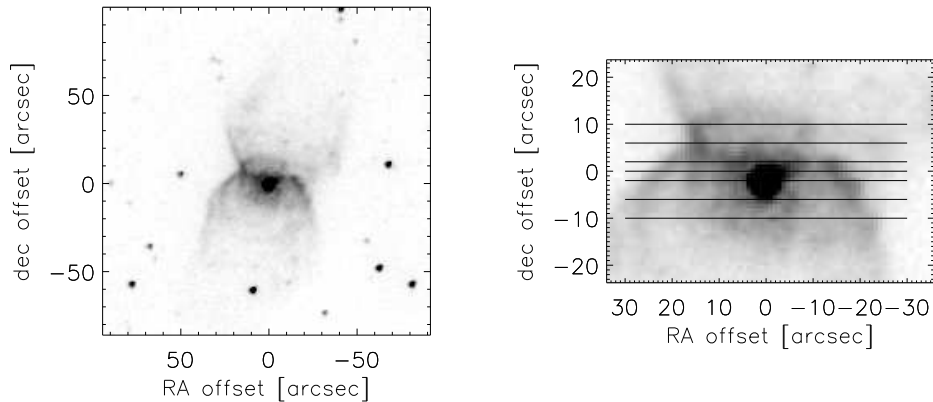


Figure 3. Left: Image of NGC 2346 in the  $2.12 \mu\text{m}$  line of  $\text{H}_2$  obtained with the NOAO Cryogenic Optical Bench (COB; Kastner et al. 1996). Right: Central region of the COB image, illustrating the slit positions used for Phoenix observations.

ring-like planetaries which display  $\text{H}_2$  are bipolar in structure (Kastner et al. 1994, 1996).

The position-velocity ellipse represented in the spectral image obtained with the slit at  $0''$  offset (leftmost panels) is noticeably tilted, with the largest redshifts found  $\sim 15''$  to the east and the largest blueshifts  $\sim 15''$  to the west of the central star. It is apparent from Fig. 3 that this tilt is due to the orientation of the Phoenix slit with respect to the object. That is, to the east of the star the slit takes in portions of the rearward-facing (redshifted) south polar lobe of the nebula, whereas to the west the slit samples portions of the forward-facing (blueshifted) north polar lobe.

Furthermore, the position-velocity ellipses in Fig. 4 contain two distinct kinematic components: a central ring associated with lower velocity material in the nebular waist and a pair of rings associated with higher velocity material in the bipolar outflow lobes. The central ring is centered at the systemic velocity of the nebula and is most apparent in the spectral images obtained near the position of the central star (i.e., in the four lefthand panels). The southern ring is primarily redshifted (righthand bottom panels) while the northern ring (righthand top panels) is primarily blueshifted. All three rings are present in the images obtained nearest the position of the central star (lefthand panels), whereas the images obtained further from the central star display emission from only a portion of the central ring and one of the outer rings. Hence Figs. 3 and 4 indicate that the  $\text{H}_2$  emission from the nebula's waist produces the inner position-velocity ring, while the outer rings arise from  $\text{H}_2$  emission from the polar

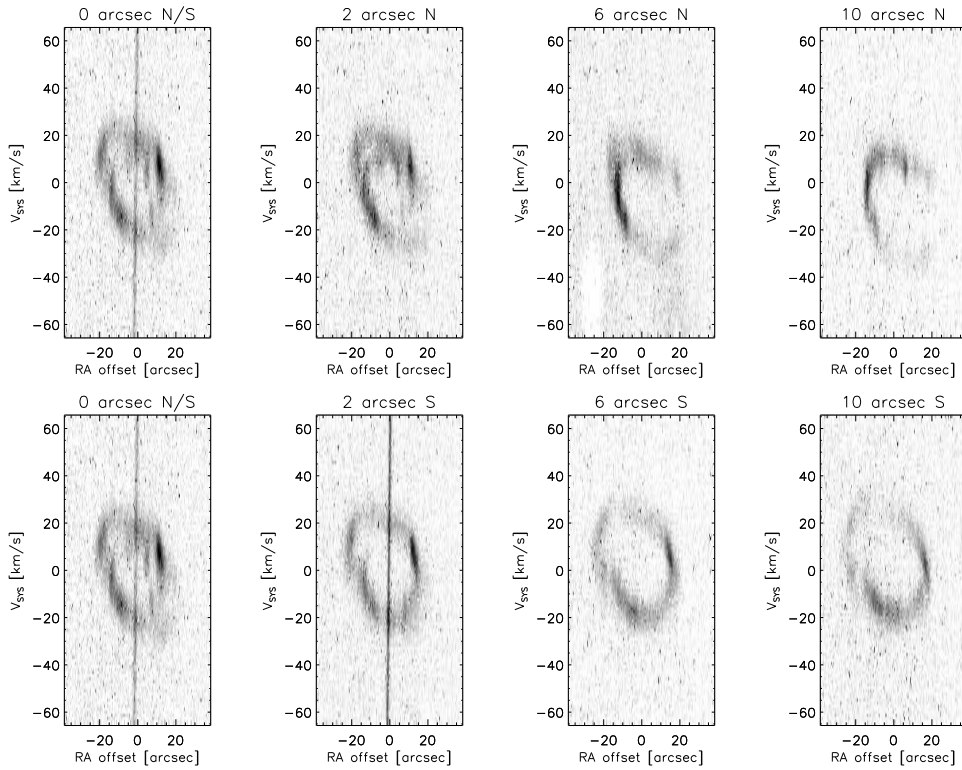


Figure 4. Phoenix position-velocity images of NGC 2346 obtained at the slit positions illustrated in Fig. 3. Top panels: images obtained as the slit was stepped northward. Bottom panels: images obtained as the slit was stepped southward. The image in the leftmost panels in each series was obtained with the slit centered on the waist of the nebula. The vertical band across the images at offsets of  $0''$  and  $2''$ S is continuum emission from the binary companion to the central star (see Bond, these proceedings).

lobes. Because of the tilt of the slit with respect to the waist of the nebula, a given slit position samples both the waist region and one or both polar lobes, resulting in a superposition of these kinematic features in a given spectral image.

In summary, the Phoenix spectral images of NGC 2346 provide strong evidence for distinct kinematic components in this nebula. These components consist of an equatorial ring or disk which is expanding at relatively low velocity ( $\sim 15 \text{ km s}^{-1}$  projected along our line of sight; Fig. 4, leftmost panels) and polar lobes that are expanding at larger velocities (Fig. 4, rightmost panels). Put differently, the equatorial confinement that is apparent in the morphology of this classical bipolar PN has a direct kinematic counterpart. It is tempting, therefore, to conclude that the pinched waist of NGC 2346 has its roots in processes which we are now beginning to explore in objects such as RAFGL 2688.

**Acknowledgments.** J.H.K. acknowledges support from a JPL Infrared Space Observatory grant to RIT. LeeAnn Henn (MIT) reduced many of the Phoenix spectral images used in this study.

## References

- Cox, P., et al. 1997, *A&A*, 321, 907
- Kastner, J.H., Gatley, I., Merrill, K.M., Probst, R.P., & Weintraub, D.A. 1994, *ApJ*, 421, 600
- Kastner, J.H., Weintraub, D.A., Gatley, I., Merrill, K.M., & Probst, R.P. 1996, *ApJ*, 462, 777
- Kastner, J.H., Henn, L., Weintraub, D.A., & Gatley, I. 1999, in *IAU Symp.* 191, "Asymptotic Giant Branch Stars," eds. T. LeBertre, A. Lebre, & C. Waelkens, p. 431
- Latter, W. B., Kelly, D. M., Hora, J. L., & Deutsch, L. K. 1995, *ApJS*, 100, 159
- Sahai, R., Hines, D., Kastner, J.H., Weintraub, D.A., Trauger, J.T., Rieke, M.J., Thompson, R.I., & Schneider, G. 1998, *ApJ*, 492, 163L
- Weintraub, D.A., Huard, T., Kastner, J.H., & Gatley, I. 1998, *ApJ*, 509, 728
- Zuckerman, B., & Gatley, I. 1988, *ApJ*, 324, 501